A Train-Borne Laser Vibrometer Solution Based on Multisignal Fusion for Self-Contained Railway Track Monitoring

Yuanchen Zeng , *Member, IEEE*, Alfredo Núñez , *Senior Member, IEEE*, Rolf Dollevoet ,
Arjen Zoeteman, and Zili Li

Abstract—This article develops and tests a self-contained railway track monitoring system that fits in existing vehicles without the need for speed and load control. Combining a train-borne laser Doppler vibrometer and axle box accelerometers enables synchronized measurements of train-track response under operational conditions. Utilizing a GPS antenna and video camera, we propose the multisignal processing method to obtain train-track vibrations with train position and speed. Then, we fuse the multiple signals to extract an impact index and a resonance index and further propose an interpretable anomaly detection strategy. We test the system on an operational line at 20–60 km/h under different working conditions and verify the detection results using information from conventional technologies. The impact index peaks near joints and welds, and the resonance index yields a good correlation with the measured track geometry. The developed solution achieves the detection, localization, and quantification of surface and support anomalies in railway tracks.

Index Terms—Anomaly detection, axle box accelerometer (ABA), laser doppler vibrometer (LDV), railway track, sensor fusion, structural health monitoring.

I. INTRODUCTION

INTELLIGENT maintenance of rail infrastructure requires effective condition monitoring technologies. Train-borne technologies enable railways to be inspected by sensors on moving trains, possibly at normal traffic speeds, thus allowing large-scale monitoring of railway tracks.

Many train-borne technologies are developed to measure the static or geometric properties of railway tracks, such as rail profile measurement using laser or structured light scanners [1], rail defect detection using eddy current or ultrasound [2], [3], and track surface inspection using machine vision [4], [5]. Track geometry describes the overall geometric deviation of the two rails along a track. It can be measured by track recording cars with various surveying methods. The chord method measures the sagitta of a chord to estimate the alignment [6]. The inertial method measures the motions of wheels to estimate the track geometry [7]. The laser distance sensor-based method scans rail heads and measures their positions along tracks [8].

Beyond the geometrical properties, the dynamic properties of railway tracks characterize how track structures respond to excitations from moving trains. Due to train loading and aging, these properties degrade in different forms, such as hanging sleepers and ballast fouling. These anomalies usually become more pronounced under moving train loads. Track stiffness measurement vehicles are developed to apply quasi-static loads to tracks, measure the track deflection, and estimate the track stiffness [9], [10]. Some vehicles can also apply oscillatory loads and measure the dynamic stiffness of railway tracks but only at a single frequency at a time [11], [12]. The running speeds of these vehicles are usually limited (e.g., below 60 km/h [11]) to control the applied wheel loads.

Most train-borne technologies require specialized vehicles due to the size of the equipment, the complexity of the configuration, and the need for speed and/or load control, so they are generally expensive to manufacture, operate, and maintain. Their availability and measurement costs limit the frequency of measurements, for example, to a few times a year. This causes significant gaps in characterizing the continuous degradation of railway tracks and hinders the timely detection of anomalies and the optimal maintenance of railway tracks.

A. Related Work

Alternatively, train-borne monitoring technologies that are compatible with various existing vehicles are being developed through the use of compact sensing techniques and the analysis of data acquired under operational loads and speeds. They allow many in-service vehicles to be instrumented, thus enabling frequent measurements and providing a wealth of information to support track maintenance decisions.

Axle box accelerometer (ABA) is a typical example of such technologies that can be mounted on the axle boxes of various types of trains. Wheel passage over anomalies in railway tracks can affect the vibration response on axle boxes through wheel-rail contact, enabling these anomalies to be detected from ABA signals. ABAs have been successfully applied to

This article has been accepted for inclusion in a future issue of this journal. Content is final as presented, with the exception of pagination.

2   IEEE TRANSACTIONS ON INDUSTRIAL INFORMATICS
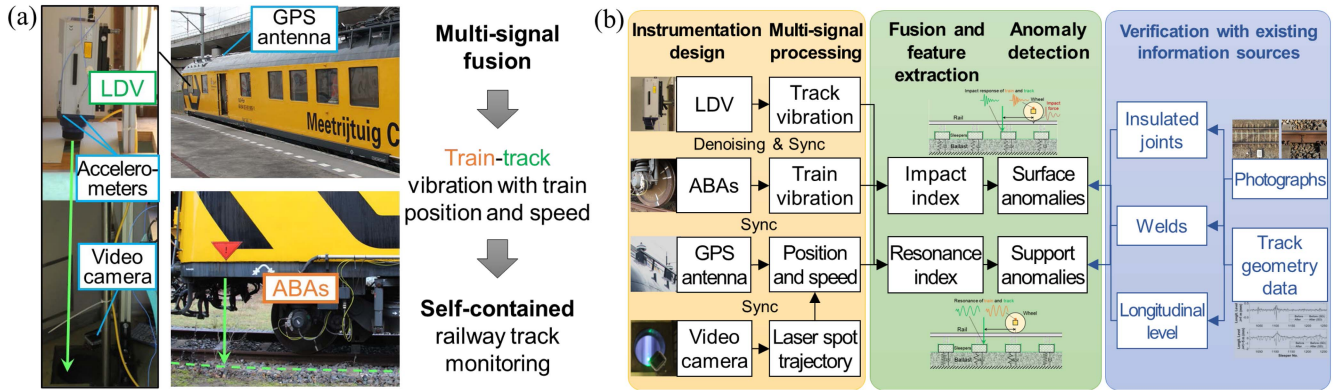

Fig. 1.   Train-borne LDV and ABAs with multisignal fusion for self-contained track monitoring. (a) Field implementation. (b) Research framework.

detecting squats, corrugation, and degraded joints and welds [13], [14], [15]. They are recently employed to identify track stiffness and detect track support anomalies [16], [17], [18], [19], [20], [21], which still require further testing. In general, ABA measurements are more effective in detecting anomalies on rails due to their high sensitivity to wheel-rail contact. In cases of using ABAs to indirectly monitor track layers below rails, significant uncertainties arise since their responses decay and mix with those of other train-track components.

A more effective solution for monitoring track layers below rails is to measure their vibrations directly. A train-borne laser Doppler vibrometer (LDV) can fulfill this need by pointing its laser spot onto tracks, scanning the track as the train moves, and measuring the track vibration in response to the moving train. It allows contactless and continuous vibration measurement on rails [22], [23], [24] or on components underneath rails, such as sleepers [25], thus providing pure information about the dynamic behavior of track structures. However, the application of train-borne LDV technology must overcome many crucial challenges, including the severe speckle noise during laser scanning on rough surfaces [26], [27] as well as the ever-changing but unknown dynamic train loads to track structures.

B. Innovation and Challenges

Both ABA and train-borne LDV are compatible with existing vehicles, but each has limitations when used independently. Essentially, ABA and train-borne LDV measure vehicle and track vibrations, respectively, with each being sensitive to certain dynamic behaviors and influenced by unknown and uncertain factors of the other. Given that vehicle and track vibrations are coupled through vehicle-track dynamics, this article combines ABA and train-borne LDV to achieve simultaneous measurements of train-track response from an operational train, as shown in Fig. 1(a). This combination offers a more comprehensive representation of train-track dynamic behavior, thus potentially improving the assessment of track dynamic properties. We are unaware of existing literature that integrates these two sensing technologies on a moving train for monitoring railway tracks.

There are many challenges in integrating and applying train-borne LDV and ABA technologies on existing vehicles for monitoring railway tracks, including following.

1) Proper instrumentation design and signal processing are needed to mitigate speckle noise in LDV signals and obtain train-track vibrations with accurate position and speed information. This can reduce disturbances and avoid reliance on external signals, thus allowing the system to be self-contained.

2) A robust fusion of ABA and LDV signals is needed to characterize train-track response under varying train speeds and uncontrolled wheel loads. Effective feature extraction can provide users with straightforward and quantitative indices for anomaly detection.

3) Comprehensive field tests are needed to evaluate the effectiveness and robustness of this new technology in the real world. To demonstrate the value of this new solution, the monitoring results need to be compared with existing methods and also verified with railway track information from various reference technologies.

C. Contributions

This article combines train-borne LDV and ABA technologies and develops a self-contained railway track monitoring system that fits in existing vehicles without the need for speed and load control. Fig. 1(b) shows the framework of this research. The aforementioned challenges are addressed by fusing multiple signals into interpretable indices for anomaly detection. Existing methods in the literature are included for a comparative study, and information from conventional technologies is used to verify the detection results. The contributions are given as follows.

1) We instrument an existing train with LDV, ABAs, a GPS antenna, and a video camera with the laser spot targeted on sleepers and ballast. A multisignal processing method is developed to obtain synchronized train-track vibrations with the train position and speed information.

2) We fuse the multiple signals and extract two interpretable features (impact and resonance indices) that characterize the dynamic train-track response and indicate anomalies. The two features have different sensitivities to various anomalies and the adaptability to varying train speeds.

3) We test the system on four different track sections of an operational railway line at the speed of 20–60 km/h over a period of two years. The combination of LDV and ABA provides condensed information and complementary performance, and the detection results are verified using track geometry data and photographs. The results demonstrate

This article has been accepted for inclusion in a future issue of this journal. Content is final as presented, with the exception of pagination.

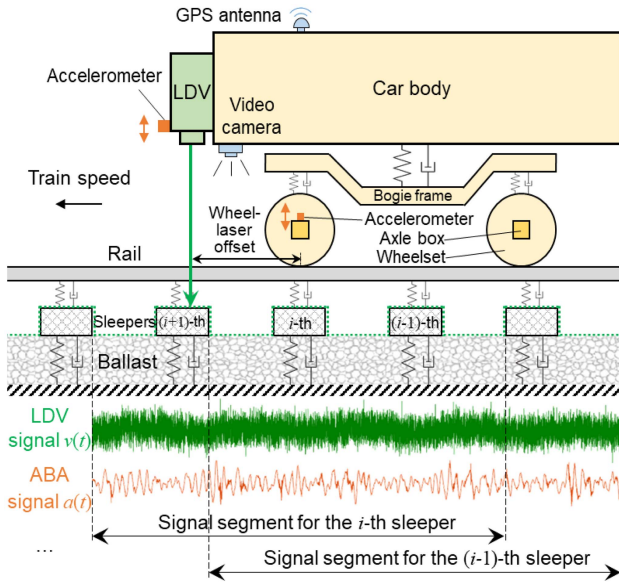ZENG et al.: TRAIN-BORNE LASER VIBROMETER SOLUTION

3

Fig. 2.   Self-contained instrumentation.

its effectiveness and robustness in detecting, localizing, and quantifying various surface and support anomalies and capturing their degradation over time.

The rest of this article is organized as follows. Section II presents the instrumentation design and the multisignal fusion method. Section III presents the field test setup and result. Section IV presents the verification for detecting various anomalies. Finally, Section V concludes this article.

II. PROPOSED METHOD

A. Self-Contained Instrumentation and Signal Processing

Fig. 2 illustrates the proposed train-borne track monitoring system. The train typically consists of a car body, bogie frames, and wheelsets. The track typically consists of rails clamped by fasteners to sleepers, which are further supported by a ballast bed made of crushed stones. An LDV is mounted on the car body with its laser spot pointed downward onto the track. Vertical vibration of the sleeper and ballast is measured as it is considered to be sensitive to track dynamic properties. An accelerometer is attached to the LDV to measure its vibration in the direction of the laser beam. Meanwhile, the wheelset closest to the LDV is instrumented with ABAs on both the left and right sides to measure the accelerations in the vertical direction. Additionally, a GPS antenna is mounted to record the position of the train, and a video camera is mounted to record the trajectory of the laser spot on the track surface.

The proposed instrumentation involves a variety of sensing devices that may have different sampling rates and separate data acquisition and storage. Therefore, proper synchronization is necessary so that the time-domain information can be correlated with the spatial domain. In this way, the system can avoid reliance on external signals, thus being self-contained. After the synchronization, all signals are then segmented around each sleeper, as shown in Fig. 2. The segment length should not be too short; otherwise, the frequency resolution would

be insufficient. The segment length should not be too long either; otherwise, local variations in track properties cannot be distinguished. Furthermore, the train speed can be estimated from the GPS signal or the video frames. The procedure of synchronization, segmentation, and speed estimation is given as follows.

Step A1: Determine the time range corresponding to the target track section according to the GPS signal. Cut the multiple signals with the same time range.

Step A2: Determine from the signals some unique objects on the track that are visible in the multiple signals (e.g., joints, crossings, and bridges). Align the multiple signals using their features at these reference locations. Average the alignments at different reference locations.

Step A3: Divide the LDV and accelerometer signals into overlapping segments based on the position of the instrumented wheelset. Each segment is centered around a sleeper and covers a certain length of the track. Denote the LDV signal segment as $v_i(t)$, the ABA signal segment as $a_i(t)$, and the signal segment of the accelerometer on the LDV as $w_i(t)$.

Step A4: Estimate the train speed for each segment based on the GPS signal or the time length passing each sleeper spacing recorded in the video camera. Denote the train speed centered at the ith sleeper as V_i.

The proposed instrumentation utilizes GPS and video camera data for synchronization, segmentation, and speed estimation. While GPS provides coarse position information (not precise enough to pinpoint each sleeper position), the video camera offers fine positioning and serves as a backup in case of GPS signal loss. Although this is effective in most situations, there remains a possibility of signal loss, such as in tunnel environments. To address this problem, we propose to utilize the sleeper passage component in ABA signals [21] for positioning and speed estimation. This solution ensures the completeness of information with the existing instrumentation, highlighting the integrity of the proposed system.

In signals measured by a train-borne LDV, speckle noise is inevitable [26], and its characteristics vary significantly for different train speeds. Meanwhile, the vibration of the LDV in the laser beam direction induces an additional component in the LDV signal. Therefore, proper signal processing is needed to mitigate the speckle noise and compensate for the LDV vibration. We adopt a speed-adaptive despeckle method in [25], and the main signal processing steps are given as follows. The details and the selection of the parameters can be found in [25].

Step B1: Apply Haar discrete wavelet transform to $v_i(t)$ and reconstruct the detail coefficient. Label a certain percentage of points in $v_i(t)$ with the largest absolute value of the reconstructed detail coefficient as spikes.

Step B2: Train a time series model with $v_i(t)$. Replace the labeled points with predictions from the model along the forward direction. Repeat the training and replacement along the inverse direction. Take the weighted average between the replacements as the imputed signal $r_i(t)$.

Step B3: Convert $w_i(t)$ from acceleration to velocity through integration and subtract it from $r_i(t)$, resulting in the track vibration velocity $y_i(t)$ centered at the ith sleeper

$$y_i(t) = r_i(t) - \int w_i(t)\, dt. \tag{1}$$

This article has been accepted for inclusion in a future issue of this journal. Content is final as presented, with the exception of pagination.

4   IEEE TRANSACTIONS ON INDUSTRIAL INFORMATICS
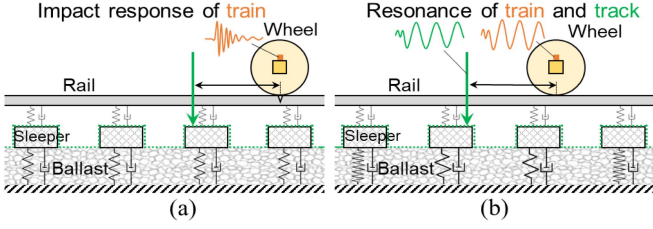

Fig. 3. Train-track vibrations on different track anomalies. (a) Surface anomalies. (b) Support anomalies.

B. Multisignal Fusion and Feature Extraction

In the proposed railway track monitoring system, the LDV measures the track vibration, while the ABAs measure the train vibration. As the train moves along a track, the train-track responses vary due to variations in track dynamic properties. Therefore, train-track vibrations measured by the LDV and ABAs can be used to assess the conditions of railway tracks.

Specifically, two common types of track anomalies can cause local variations in train-track vibrations—surface anomalies (e.g., joints, welds, and rail surface defects) and support anomalies (e.g., ballast fouling and hanging sleepers). Fig. 3 illustrates the train-track vibration responses on different anomalies. When a wheel runs over an anomaly on the rail surface, an impact force is generated between the wheel and rail, and the train vibration measured by the ABA exhibits an impact response that is typically broadband and transient [13], [15]. When a train runs over a local change in track support, both the train and track experience local changes in the vibration amplitudes and frequencies [28], which is called "resonance" in this article. Support anomalies generally have longer wavelengths and lower frequencies than surface anomalies. These two types of anomalies can develop independently, while they can also deteriorate each other.

To capture variations in train-track vibrations and distinguish between different types of track anomalies, we correlate the LDV and ABA signals and extract two features—an impact index and a resonance index. They are calculated for each track segment based on power spectral density (PSD) analysis. Cross PSD is selected to decompose the correlation of the LDV and ABA signals in the frequency domain, thus capturing the train-track resonance and supporting interpretable feature extraction. Since train speed affects the frequency and amplitude of train-track vibrations, normalization with the speed is necessary. The steps of multisignal fusion and feature extraction are given below.

Step C1: Convert axle box acceleration $a_i(t)$ to vibration velocity $x_i(t)$ through frequency-domain integration

$$x_i(t) = \int a_i(t)\, dt. \tag{2}$$

Step C2: Estimate the PSD of $x_i(t)$ and the cross PSD of $y_i(t)$ and $x_i(t)$, resulting in $P_i(f)$ and $P_{ci}(f)$, respectively,

$$P_i(f) = \int \left(\int x_i(t)\, x_i(t-\tau)\, dt \right) e^{-j2\pi f\tau}\, d\tau \tag{3}$$

$$P_{ci}(f) = \int \left(\int x_i(t)\, y_i(t-\tau)\, dt \right) e^{-j2\pi f\tau}\, d\tau \tag{4}$$

where τ represents the time lag, j represents the imaginary unit, and f represents the frequency in Hertz.

Step C3: Normalize f to spatial frequency f_s in m^{-1} with the train speed V_i as follows:

$$f_s = \frac{f}{V_i}. \tag{5}$$

Step C4: Average $|P_i(f_s)|$ within a high-frequency range ($f_{sc} < f_s < f_{su}$) as follows, where f_{sc} and f_{su} are the limits of the frequency range and n_{fp} is the number of discrete frequencies within this range

$$p(i) = \frac{\sum_{f_{sc} < f_s < f_{su}} |P_i(f_s)|}{n_{fp}}. \tag{6}$$

Then, normalize $p(i)$ with the train speed V_i as follows to calculate an impact index, denoted as $I_p(i)$

$$I_p(i) = \frac{p(i)}{V_i}. \tag{7}$$

Step C5: Average $|P_{ci}(f_s)|$ within a low-frequency range ($f_{sl} < f_s < f_{sc}$) is as follows, where f_{sl} and f_{sc} are the limits of the frequency range, and n_{fr} is the number of discrete frequencies within this range

$$r(i) = \frac{\sum_{f_{sl} < f_s < f_{sc}} |P_{ci}(f_s)|}{n_{fr}}. \tag{8}$$

Then, average $r(i)$ among adjacent $2n_s+1$ tracks segments and normalizes the result with the train speed V_i as follows to calculate a resonance index, denoted as $I_r(i)$:

$$I_r(i) = \frac{\sum_{j=i-n_s}^{i+n_s} r(j)}{(2n_s + 1) V_i}. \tag{9}$$

In the above procedure, we use different frequency and spatial ranges to capture different dynamic behaviors of the train and track, so that the two features have different sensitivities to various anomalies. For the impact index I_p, we use the PSD of $x_i(t)$ at high frequencies to capture the transient and broadband impact response of the train in each track segment. For the resonance index I_r, we use the cross PSD of $y_i(t)$ and $x_i(t)$, a frequency-domain representation of the correlation between the LDV and ABA signals, to indicate the train-track resonance. The cross PSD at low frequencies is further averaged among adjacent track segments since such resonance is considered to have longer wavelengths. For a certain track segment, a larger I_p indicates a more significant train impact response, while a larger I_r indicates a more significant train-track resonance. These steps ensure the interpretability of the extracted features.

Moreover, the influence of the train speed is normalized in both the frequency and amplitude, which provides adaptability to varying train speeds. Thus, the two indices enable the train-track dynamics to be characterized along railway tracks despite varying operating conditions. As an overview of the proposed method, its flowchart is shown in Fig. 4.

C. Anomaly Detection

We further utilize the two interpretable indices to detect surface and support anomalies. The strategy is illustrated in Fig. 5, in which I_p and I_r are compared among track segments along a track. Track segments exhibiting both small I_p and I_r are considered normal or healthy. Large I_p suggests the existence of surface anomalies that cause train impact response. Large
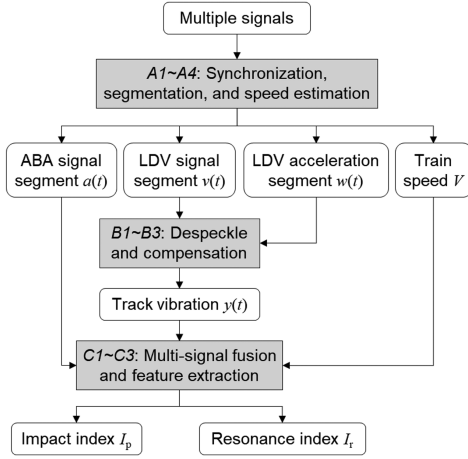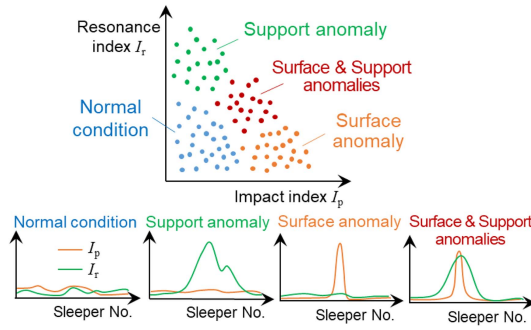
Fig. 4. Flowchart of the proposed method.

Fig. 5. Anomaly detection based on the two interpretable features.

I_r suggests the existence of support anomalies that cause train-track resonance. Track segments with both large I_p and large I_r suggest the co-existence of surface and support anomalies. Meanwhile, the larger the I_p or I_r, the more severe the surface or support anomaly. It should be noted that effective anomaly detection requires comparisons among a sufficient amount of track segments with the same structural design. The proposed strategy is capable of localizing, distinguishing, and quantifying surface and support anomalies.

Furthermore, the above indices can be calculated using signals from the left ABA and the right ABA separately, producing the indices for both sides of the track. This allows the further localization of anomalies, which may occur on the left, right, or both sides of the track.

III. FIELD TEST ON AN EXISTING TRAIN

A. Measurement Campaigns

We implement the proposed instrumentation on the CTO measurement train of TU Delft, as shown in Fig. 1(a). An LDV is installed in the cabin, and its laser beam is pointed onto the track through a hole in the cabin floor. Two accelerometers are attached to the LDV to measure its vibration. A video camera is mounted next to the hole, and a GPS antenna is mounted on the roof of the train. Meanwhile, ABAs are installed on the left and right axle boxes of the first wheelset. The LDV and the accelerometers use a sampling rate of 102.4 kHz. The GPS module produces one train position per second, and the video camera
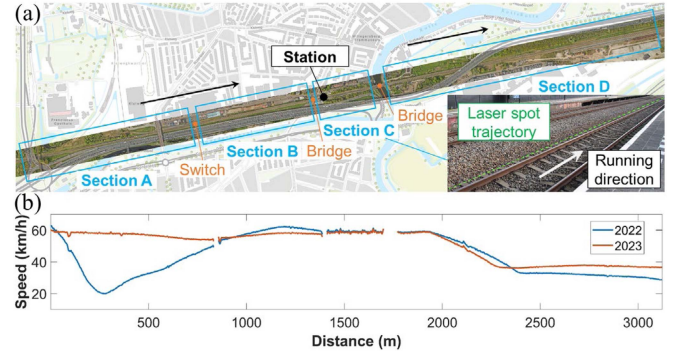

Fig. 6. Field measurements. (a) Selected track sections (source of aerial photograph: ProRail geoinformation portal). (b) Speed profiles of the two measurements.

produces 240 frames per s. Considering the separate acquisition and storage, we synchronize the GPS signal, the video frames, and the vibration signals according to Step A1–A2.

We conduct field measurements on an operational railway track in The Netherlands that supports single-directional traffic. It is a ballasted track with concrete sleepers spaced at an interval of 0.6 m. Four different track sections, namely Sections A–D, are selected for our case study, as shown in Fig. 6(a). Switches and bridges are excluded since they have different track structures. The lengths of the four-track sections are around 830, 535, 290, and 1355 m, respectively. Section C is located at a station.

Two measurement campaigns were conducted in May 2022 and May 2023, respectively. The train speed profiles were different, as shown in Fig. 6(b), where the train speed is estimated under the assumption of uniform sleeper spacing. The speeds on the four track sections range from 20 to 60 km/h. Some sections exhibit significant variations, such as Section A in 2022, while others have more stable speed profiles. The weather conditions were also different: it was sunny during the one in 2022, whereas the track surface was wet due to rain during the other in 2023. These two measurements allow us to investigate the degradation of the track structure and the performance of the system in different operational conditions.

B. PSD Spectra on Different Track Sections

According to Step A3, we cut the multiple signals into segments centered around each sleeper and covering three sleepers. We apply Step A4, B1–B3, and C1–C2 to obtain the PSD of the LDV and ABA signals. Fig. 7 shows the result for Section A measured in 2022, in which the spectrum of each track segment is represented by a colored bar and indexed by the sleeper number. The ABA spectra exhibit a belt at the frequency of sleeper passage, which can be useful for positioning and speed estimation (mentioned in Section II-A). Several transient and broadband peak bars can also be observed, indicating the impact response of the wheel. In contrast, the LDV spectra exhibit much more pronounced components at low frequencies. These results reflect the different sensitivities of the two sensing technologies to different dynamic behaviors, which are considered complementary in monitoring track conditions. It is also noteworthy that, as the train speed varies between 20 and 60 km/h (shown in Fig. 6), the PSD results of the ABA and LDV show significant speed-dependent characteristics in both their amplitudes and

This article has been accepted for inclusion in a future issue of this journal. Content is final as presented, with the exception of pagination.

6   IEEE TRANSACTIONS ON INDUSTRIAL INFORMATICS
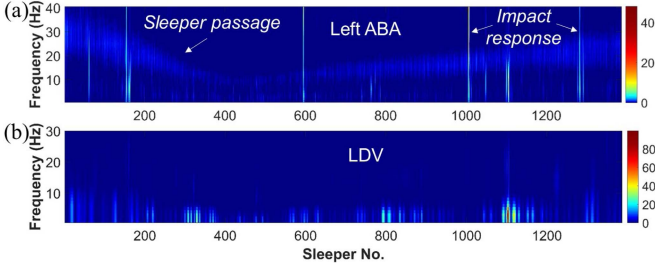
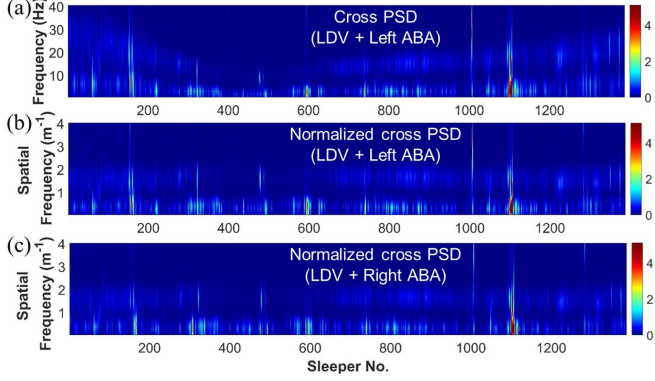Fig. 7.   PSD results on Section A in 2022. (a) Left ABA. (b) LDV.

Fig. 8.   Cross PSD results on Section A in 2022. (a) Cross PSD of the left ABA and the LDV. (b) Normalized cross PSD of the left ABA and the LDV. (c) Normalized cross PSD of the right ABA and the LDV.

frequencies. The frequency and amplitude generally increase with the increasing speed.

The cross PSD spectra of the left ABA and the LDV are plotted in Fig. 8(a). It can be seen that the cross PSD combines the patterns of the ABA and LDV spectra and enhances the peak regions where both the ABA and LDV spectra exhibit large amplitudes as they yield high correlation. This reflects the ability of the method to fuse the multiple signals and provide more condensed information than either can provide alone. Further, we normalize the frequency by the train speed according to Step C3, as shown in Fig. 8(b), in which the spatial frequency is no longer dependent on the train speed. Meanwhile, variations in the cross PSD along the track can be observed, and larger ampli-tudes indicate more significant train-track resonance at certain frequencies and locations. Fig. 8(c) further plots the normalized cross PSD of the right ABA and the LDV. Both similarities and differences can be observed by comparing Fig. 8(b) and (c), reflecting the correlation and deviation in the train-track response between the left and right sides of the same track.

The same calculation is also applied to Section B–D. Fig. 9 plots the results of Section C, in which the same color mapping as Fig. 8 is used. Section C exhibits more dense peak regions than Section A, and the left side exhibits more peaks than the right side. These results show the potential of the normalized cross PSD to reflect variations in train-track resonance along a track or between the two sides of a track.

C. Indices on Different Track Sections

We further apply Step C4–C5 to the PSD results and calculate the impact index I_p and the resonance index I_r for each track
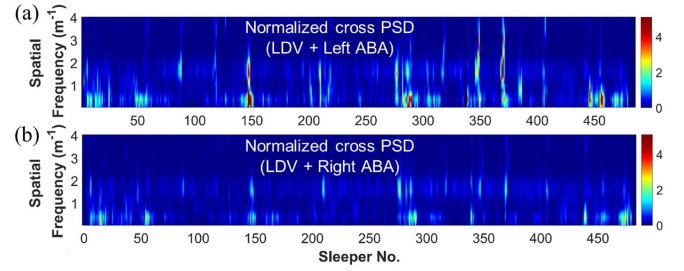

Fig. 9.   Normalized cross PSD results on Section C in 2022. (a) Left ABA and the LDV. (b) Right ABA and the LDV.
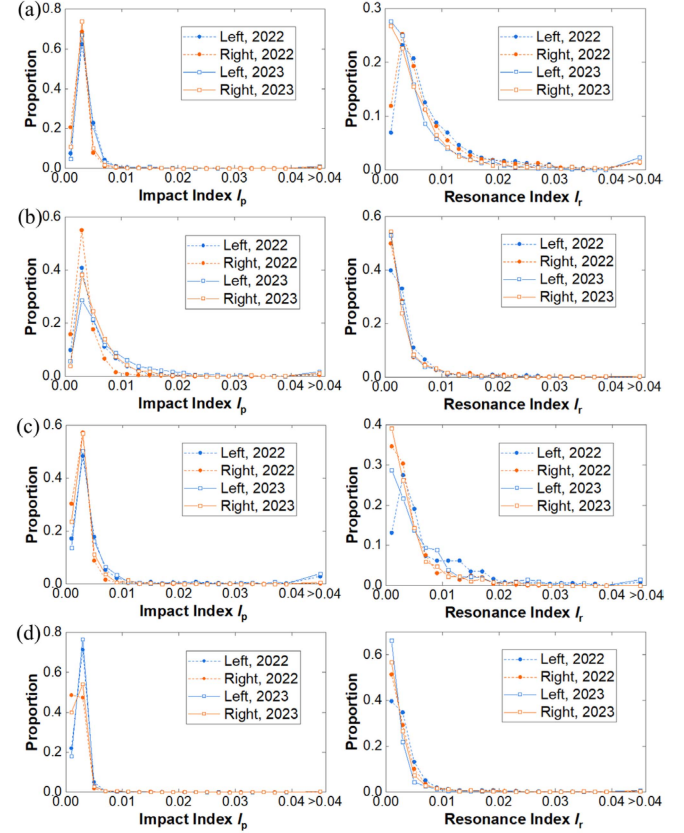

Fig. 10.   Distributions of the two indices from the two measurements. (a) Section A. (b) Section B. (c) Section C. (d) Section D.

segment. We use the cut-off spatial frequencies of $f_{sc} = 1$ m^{-1}, $f_{sl} = 0.05$ m^{-1}, and $f_{su} = 4$ m^{-1}, and the number of adjacent track segments for averaging is $n_s = 2$. Fig. 10 shows the distributions of I_p and I_r on each track section over the two years, and the first two rows of Table I show the correlation coefficients between the two measurements (0.78 on average). Generally, the two measurements yield good repeatability. It is noteworthy that the two measurements in Section A yield a high correlation (0.83 on average) despite their significant difference in train speeds (shown in Fig. 6), which demonstrates the adaptability of the system across different operational conditions. Most of the indices are small, corresponding to normal conditions, whereas the minority with large values indicates possible anomalies.

The distribution of I_p is similar on different track sections. The left rail of Section C exhibits a higher proportion of $I_p > 0.04$ than the others, indicating denser surface anomalies. From 2022

TABLE I
CORRELATION COEFFICIENTS BETWEEN DIFFERENT YEARS AND SOURCES

		Section A	Section B	Section C	Section D
Correlation between 2022 and 2023	I_p	0.866	0.756	0.554	0.915
	I_r	0.794	0.722	0.741	0.858
Correlation between I_r and longitudinal level in 2022	$\lambda = 1$ m	0.575	0.674	0.620	0.537
	$\lambda = 1{\sim}5$ m	0.448	0.542	0.418	0.437
	$\lambda = 3{\sim}25$ m	0.374	0.351	0.234	0.440
Correlation between I_r and longitudinal level in 2023	$\lambda = 1$ m	0.454	0.759	0.649	0.623
	$\lambda = 1{\sim}5$ m	0.512	0.646	0.430	0.501
	$\lambda = 3{\sim}25$ m	0.403	0.367	0.244	0.434

to 2023, the proportion of $I_p > 0.005$ increases on both rails of Section B, indicating the degradation of its surface anomalies. The distribution of I_r shows more diversity among different track sections, reflecting their different conditions. Both sides of Section A and the left side of Section C have a higher proportion of $I_r > 0.01$ than the other sections. Such differences can be also observed in Figs. 8 and 9. Detailed findings on the four sections will be shown further.

IV. VERIFICATION AND COMPARISON

In this section, we first verify the anomaly detection results by comparing them with available information from conventional track geometry measurements and photographs. Then, we compare our developed method with existing methods in the literature to discuss their pros and cons.

A. Correlation With Longitudinal Level

The track geometry measurement data were acquired by specialized track recording cars in three months over the two years—Feb. 2022, Aug. 2022, and Jul. 2023. The longitudinal level of the left and right rails is adopted, which refers to the vertical deviation of the rail top along the track [29]. The data are provided with a spatial interval of 0.25 m and defined within different wavelength (λ) ranges. We focus on the wavelength below 25 m and calculate the standard deviation of the longitudinal level within a moving window of 3 m, which is generally related to the condition of track support [29].

For each track section measured in each year, we align the resonance index I_r with the standard deviation of the longitudinal level and calculate their correlation coefficients (averaged between left and right sides) in different wavelength ranges. The results in Table I show that, in general, the correlation increases as the wavelength decreases. At $\lambda = 1$ m, the correlation coefficient reaches 0.61 on average, indicating a good correlation between the two technologies. Track segments with large I_r are more likely to have large variations in longitudinal level, suggesting possible support anomalies [30]. It demonstrates the effectiveness of the proposed indices in quantifying track conditions.

It is noteworthy that such a correlation is achieved between two technologies with different measurement mechanisms and capabilities—one measures dynamic response of both long and short wavelengths, whereas the other measures geometry and smooths out short-wave components. Positioning errors between the two systems also affect their correlation. As a result, they exhibit a certain correlation but not necessarily a
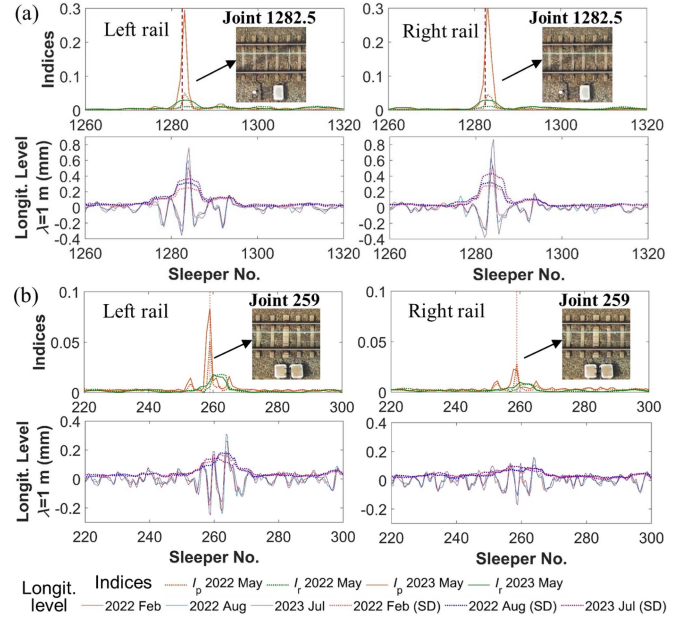
Fig. 11. Indices and longitudinal level near the joints. (a) Joint in Section A. (b) Joint in Section D. "SD" represents the standard deviation of the longitudinal level. (Source of aerial photographs: ProRail geoinformation portal).

very high coefficient, indicating their complementariness. The developed monitoring system is superior to the existing specialized track recording cars in its unique ability to measure train-track dynamics and detect short-wave anomalies, as well as in its compatibility with existing vehicles, thus providing the capability to supply missing information needed for structural health assessment and providing more intensive information.

B. Insulated Joints in Various Conditions

Insulated joints are typical surface anomalies that cause gaps and height differences between two connected rails. The passage of wheels over joints induces significant dynamic loads, which can lead to support anomalies. Due to the uniqueness of working conditions and degradation, different joints exhibit different dynamic behaviors. We select one joint in Section A and one in Section D as examples. These joints have different designs: the one in Section A is located in the middle of two normal sleepers, whereas the other in Section D is directly on top of a special wide sleeper, as shown in Fig. 11.

Fig. 11(a) shows the calculated indices and the measured longitudinal level near the joint in Section A. For both rails, the impact index I_p exhibits a peak, and the resonance index I_r is large over the joint. From 2022 to 2023, both I_p and I_r increase significantly. In the longitudinal level plots, peaks appear near the joints, and their amplitude increases with time, which confirms the degradation of track support (larger I_r) due to the increased impact load (larger I_p). This result demonstrates the effectiveness of the method in detecting the surface and support anomalies near the joint and capturing their degradation.

Fig. 11(b) shows the results near the joint in Section D. The left rail has a larger I_p and I_r than the right rail. The change in I_p and I_r between the two years is not as pronounced as the joint in Section A, which may be related to their different designs. From 2022 to 2023, the peak of I_r shifts toward the joint location,
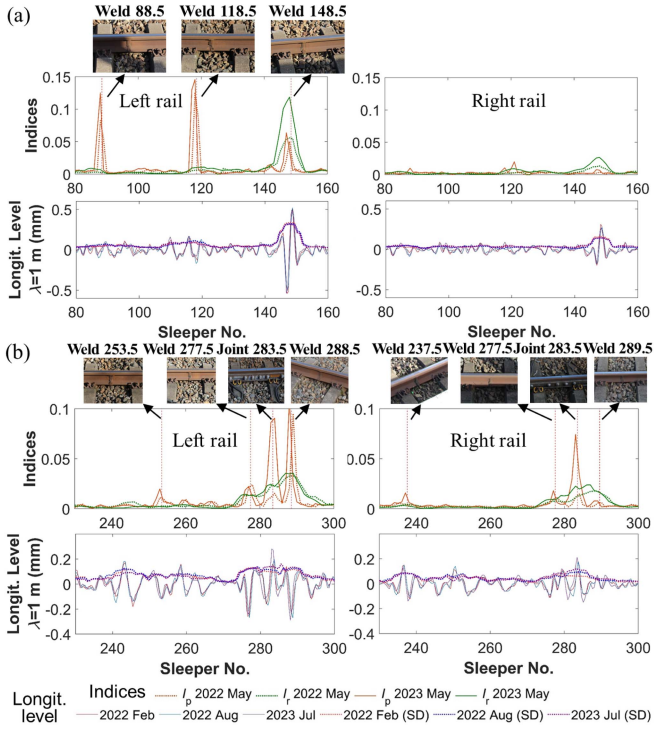
This article has been accepted for inclusion in a future issue of this journal. Content is final as presented, with the exception of pagination.

8   IEEE TRANSACTIONS ON INDUSTRIAL INFORMATICS

Fig. 12. Indices and longitudinal level near the welds in Section C. (a) Sleeper No. 80–160. (b) Sleeper No. 230–300. "SD" represents the standard deviation of the longitudinal level.

Fig. 13. Other detected anomalies in Section B. (a) Sleeper No. 250–550. (b) Sleeper No. 650–750. "SD" represents the standard deviation of the longitudinal level (source of aerial photographs: ProRail geoinformation portal). (c) Results of Sleeper No. 250–550 following the existing ABA-based methods, in which TQI-int is calculated according to [19], TKD-cum4 is calculated according to [20], and VKF-slp is calculated according to [21].

which can be confirmed by the longitudinal level plots. This shows the capability of the method to capture local variations in track conditions.

For the two joints, the co-existence of large I_r and large I_p suggests that the joints cause the degradation in track support. The track support condition degrades more (larger I_r) as a consequence of a larger impact load (larger I_p). These results demonstrate the effectiveness of the indices in assessing the surface and support conditions near joints.

C. Welds in Various Conditions

Welds are used to connect rails to form seamless long ones or when a piece of rail needs to be replaced. Poor-quality welds due to improper welding or degradation are typical rail surface anomalies in railway tracks. Welds can induce dynamic loads under wheel passage and accelerate track degradation.

Since welds are not visible from the aerial photographs, we focus on Section C where photographs of the track are taken from the station platform next to it. This section has much denser welds than normal tracks, implying more replacements on this track. This is consistent with the findings of more peaks in the cross PSD spectra in Fig. 9 as well as larger I_p and I_r in Fig. 10, reflecting the poor track conditions.

Fig. 12 shows the extracted indices covering nine welds in Section C. Significant diversity can be observed: Weld 88.5 and 118.5 exhibit large I_p but small I_r, indicating mainly surface anomalies. Weld 148.5, 277.5, 288.5, and 289.5 show both peaks of I_p and I_r, indicating the co-existence of surface and support anomalies. Weld 253.5 and 237.5 show small I_p and I_r, indicating relatively healthy conditions. Additionally, a weld on one side can cause an anomaly on the other side, such as
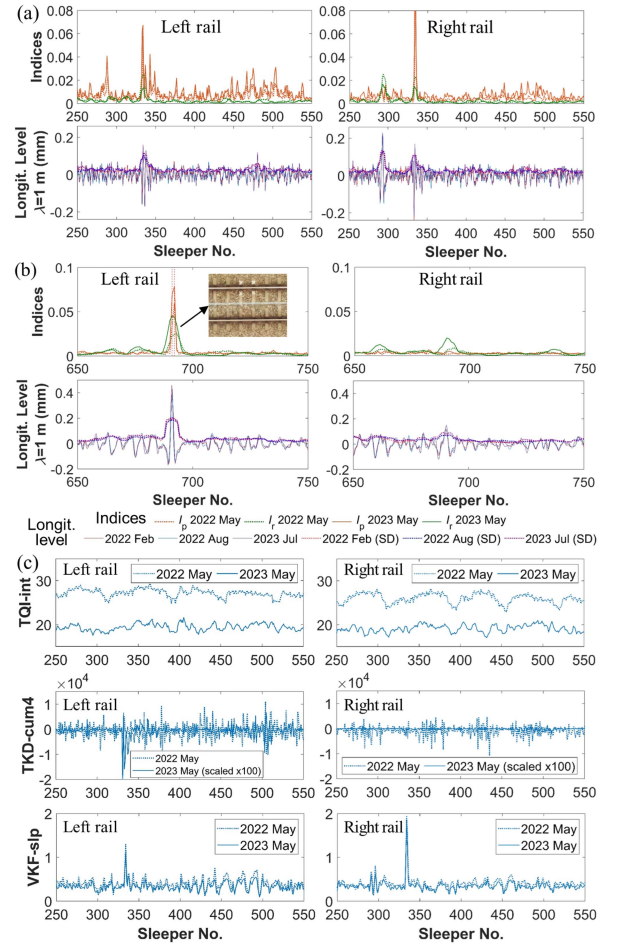
Weld 148.5. The longitudinal level verifies the track support conditions near these welds. These results demonstrate that the developed method can effectively detect and localize the surface and support anomalies near welds.

D. Other Anomalies

Fig. 13(a) and (b) shows a few other anomalies detected in Section B. Sleeper No. 334 exhibits large I_p and I_r on both rails, and Sleeper No. 293 exhibits large I_r only on the right rail. These results are consistent with the longitudinal level data, demonstrating the effectiveness of the proposed strategy in localizing anomalies. Sleeper No. 691–692 show large I_p and I_r as well as large longitudinal level, especially on the left side. In the aerial photographs, cross marks are found on the left side of these sleepers, suggesting certain track problems yet without information on the exact reason.

Moreover, Fig. 13(a) and (b) also show that locations with low I_r also have low longitudinal level, demonstrating the reliability of the method in assessing healthy or normal conditions, which are in the majority of railway networks.

TABLE II
EXISTING ABA-BASED METHODS FOR MONITORING TRACK STIFFNESS OR SUPPORT CONDITIONS

Reference	Objective	Sensors and instrumentation	Methodology	Testing condition	Further comparison
Shen, et al., 2023 [17]	Estimate track stiffness in multiple layers with ABA	Accelerometer Sampling rate: 100 kHz	Select a model from a model library based on extracted wavelet spectrum features using ABA over each sleeper	Laboratory measurements on a downscale test rig in the Netherlands (speeds: 7~13 km/h)	Not compared due to the lack of a vehicle-track model
Vishwakarma, et al., 2024 [18]	Detect rail fastener defects with ABA	Accelerometer (0.5~5k Hz) and tachometer (for speed) Sampling rate: 500 Hz	Calculate the correlation coefficient between filtered ABA and simulated template signals with defects	Simulation cases and a real field measurement case without defects in India (length: 320 m, speed: 90 km/h)	Not compared due to the lack of template signals
Chudzikiewicz, et al., 2018 [19]	Assess track overall conditions with ABA	Accelerometer and GPS (for position) Sampling rate: 12 kHz	Calculate an indicator based on the integral of the derivative of filtered ABA over each segment	Field measurements on a test track (length: 7.8 km, speed: 40~160 km/h) and operational tracks in Poland (length: 9 km)	Compared by denoting the result as TQI-int
Miao, et al., 2023 [20]	Detect ballastless track mortar layer void with ABA	Accelerometer Sampling rate: 2.5 kHz	Calculate the 4th order cumulant time-varying kurtosis difference using filtered ABA on each segment	Simulation cases and a real field measurement case with avoid areas in a high-speed line in China (speed: 300+ km/h)	Compared by denoting the result as TKD-cum4
Hoelzl, et al., 2023 [21]	Assess track overall stiffness with ABA	Accelerometer	Filter ABA signal and extract the sleeper passage amplitude over each segment	Field measurements in Switzerland (length: 30 km, speed: 0~200 km/h)	Compared by denoting the result as VKF-slp

In summary, the proposed impact index I_p and resonance index I_r are sensitive to surface and support anomalies, respectively. The proposed method allows the localization of anomalies not only to the sleeper number but also to the left or right side of the track. The two measurement campaigns with different speed profiles and operational conditions demonstrate the robustness of the monitoring system and the adaptability of the detection method.

E. Comparison With Existing Methods

In this section, the developed method is further compared with existing methods in the literature to highlight the novelty and value of combining the train-borne LDV and ABA. The comparison focuses on the monitoring of track support conditions or track stiffness, considering that the detection of rail surface defects is not the main purpose of utilizing the LDV. To the best of our knowledge, there is no published research on the use of LDV to directly monitor track support conditions or track stiffness, and the recent approaches using purely ABA for this purpose are summarized in Table II. Among these methods, the methods of [19], [20], and [21] are implemented directly on ABA signals without the need for models. To better understand the pros and cons of the different methods, they are utilized to process the ABA data in our field test.

Fig. 13(c) showcases the results calculated following the methods in [19], [20], and [21] for the same track section as Fig. 13(a). By comparing Fig. 13(c) with the longitudinal level in Fig. 13(a), it can be seen that the calculated TQI-int cannot effectively indicate the support anomalies near Sleeper No. 334 on both rails nor the one near Sleeper No. 293 on the right rail. The calculated TKD-cum4 peaks only on the left rail near Sleeper No. 334 but not on others. The calculated VKF-slp detects the anomalies near Sleeper No. 334 on both rails while exhibiting small peaks near Sleeper No. 293 on the right rail. In contrast, the calculated I_r can detect all these anomalies and provide better agreement with the longitudinal level data. It should be noted that although we implement and adapt the procedures presented in [19], [20], and [21], there are still parameters that can be further tuned to improve their performance.

Moreover, the calculated TQI-int and TKD-cum4 show low repeatability between the two years because they are calculated directly in the time domain, thus being less robust to varying factors, such as the different sensor types and positions between the two years. The calculated I_r and VKF-slp have high repeatability as they are calculated within certain frequency ranges. To further compare the computational efficiency of the different methods, their average CPU time (on Intel Xeon E5-2643) for computing the index of each sleeper is compared. It shows that the I_r (86 ms per sleeper) and VKF-slp (68 ms per sleeper) are computed much faster than the TQI-int (456 ms per sleeper) and TKD-cum4 (447 ms per sleeper).

In summary, within the scope of our case study, the developed method achieves better performance than the existing ABA-based methods. This highlights the value of employing the LDV in directly measuring track dynamics and providing features that ABA can hardly capture. Additionally, our developed system contains positioning, speed estimation, and speed normalization processes, thus considered more self-contained, whereas many existing methods still require supplementary information.

V. CONCLUSION

This article develops and tests a self-contained train-borne monitoring solution that fuses signals from the LDV, ABAs, GPS, and video camera for anomaly detection in railway tracks. The main conclusions are summarized as follows.

1) The proposed system is compatible with existing vehicles and self-contained in measuring train-track vibrations with train position and speed in operation.
2) The train-borne LDV and ABA have different sensitivities to different dynamic behaviors. The proposed combination provides a comprehensive assessment of track dynamic properties considering train-track dynamics.
3) The proposed impact index I_p and resonance index I_r are interpretable and effective features for detecting and localizing surface and support anomalies as well as quantifying their degradation over time.

4) The normalization eliminates the speed-dependent characteristics of the PSD, providing the adaptability to varying train speeds (20–60 km/h in the test).

5) The resonance index I_r yields a correlation of 0.63 with the measured longitudinal level at the wavelength of 1 m.

Future improvements will be made to make the developed technology more efficient and intelligent. The bottleneck in the current pipeline is the accurate segmentation of the multiple signals for each sleeper according to the laser spot trajectory, which can be improved by incorporating georeferencing information of track structures. Such improvements will further enhance the usability of the technology in large-scale and real-time applications.

REFERENCES

[1] J. Ye, E. Stewart, D. Zhang, Q. Chen, K. Thangaraj, and C. Roberts, "Integration of multiple sensors for noncontact rail profile measurement and inspection," *IEEE Trans. Instrum. Meas.*, vol. 70, 2021, Art. no. 7002212.

[2] L. U. Daura and G. Y. Tian, "Characterization of angular RCF cracks in a railway using modified topology of WPT-based eddy current testing," *IEEE Trans. Ind. Inform.*, vol. 19, no. 4, pp. 5612–5622, Apr. 2023.

[3] D. Bombarda, G. M. Vitetta, and G. Ferrante, "Rail diagnostics based on ultrasonic guided waves: An overview," *Appl. Sci.*, vol. 11, no. 3, Jan. 2021, Art. no. 1071.

[4] T. Yang, Y. Liu, Y. Huang, J. Liu, and S. Wang, "Symmetry-driven unsupervised abnormal object detection for railway inspection," *IEEE Trans. Ind. Inform.*, vol. 19, no. 12, pp. 11487–11498, Dec. 2023.

[5] M. Karakose and O. Yaman, "Complex fuzzy system based predictive maintenance approach in railways," *IEEE Trans. Ind. Inform.*, vol. 16, no. 9, pp. 6023–6032, Sep. 2020.

[6] A. Sánchez, J. L. Bravo, and A. González, "Estimating the accuracy of track-surveying trolley measurements for railway maintenance planning," *J. Surv. Eng.*, vol. 143, no. 1, Feb. 2017, Art. no. 05016008.

[7] X. Sun, F. Yang, J. Shi, Z. Ke, and Y. Zhou, "On-board detection of longitudinal track irregularity via axle box acceleration in HSR," *IEEE Access*, vol. 9, pp. 14025–14037, 2021.

[8] T. Hackel, D. Stein, I. Maindorfer, M. Lauer, and A. Reiterer, "Track detection in 3D laser scanning data of railway infrastructure," in *Proc. Int. Instrum. Meas. Technol. Conf.*, 2015, pp. 693–698.

[9] R. Thompson and P. Marquez, "Track strength testing using TTCI's track loading vehicle," *Railway Track Struct.*, vol. 97, no. 12, pp. 15–17, Dec. 2001.

[10] B. McVey et al., "Track modulus measurement from a moving railcar," in *Proc. AREMA Annu. Conf.*, 2005, pp. 1–33.

[11] E. Berggren, "Railway track stiffness: Dynamic measurements and evaluation for efficient maintenance," Ph.D. dissertation, Sch. Eng. Sci., KTH, Stockholm, Sweden, 2009.

[12] P. Wang, L. Wang, R. Chen, J. Xu, J. Xu, and M. Gao, "Overview and outlook on railway track stiffness measurement," *J. Modern Transp.*, vol. 24, no. 2, pp. 89–102, May 2016.

[13] Z. Li, M. Molodova, A. Núñez, and R. Dollevoet, "Improvements in axle box acceleration measurements for the detection of light squats in railway infrastructure," *IEEE Trans. Ind. Electron.*, vol. 62, no. 7, pp. 4385–4397, Jul. 2015.

[14] J. Li and H. Shi, "Rail corrugation detection of high-speed railway using wheel dynamic responses," *Shock Vib.*, vol. 2019, no. 1, Feb. 2019, Art. no. 2695647.

[15] A. Nunez, A. Jamshidi, and H. Wang, "Pareto-based maintenance decisions for regional railways with uncertain weld conditions using the Hilbert spectrum of axle box acceleration," *IEEE Trans. Ind. Inform.*, vol. 15, no. 3, pp. 1496–1507, Mar. 2019.

[16] P. Quirke, D. Cantero, E. J. OBrien, and C. Bowe, "Drive-by detection of railway track stiffness variation using in-service vehicles," in *Proc. Inst. Mech. Eng. Part F, J. Rail Rapid Transit*, 2017, pp. 498–514.

[17] C. Shen, P. Zhang, R. Dollevoet, A. Zoeteman, and Z. Li, "Evaluating railway track stiffness using axle box accelerations: A digital twin approach," *Mech. Syst. Signal Process.*, vol. 204, Dec. 2023, Art. no. 110730.

[18] A. Vishwakarma, S. K. Singh, V. Racherla, and A. Dasgupta, "Detection of rail fastener assembly defects using axle-box acceleration," *J. Vib. Eng. Technol.*, pp. 1–21, Mar. 2024, doi: 10.1007/s42417-024-01310-6.

[19] A. Chudzikiewicz, R. Bogacz, M. Kostrzewski, and R. Konowrocki, "Condition monitoring of railway track systems by using acceleration signals on wheelset axle-boxes," *Transport*, vol. 33, no. 2, pp. 555–566, Jan. 2018.

[20] S. Miao, L. Gao, F. Tong, Y. Zhong, C. Ma, and Z. Chen, "Ballastless track mortar layer void detection by high-order statistical analysis of axle box acceleration," *Measurement*, vol. 211, Apr. 2023, Art. no. 112681.

[21] C. A. Hoelzl, V. Dertimanis, L. Ancu, A. Kollros, and E. Chatzi, "Vold-Kalman filter order tracking of axle box accelerations for railway stiffness assessment," *Mech. Syst. Signal Process.*, vol. 204, Dec. 2023, Art. no. 110817.

[22] K. Kaynardag, G. Battaglia, A. Ebrahimkhanlou, A. Pirrotta, and S. Salamone, "Identification of bending modes of vibration in rails by a laser doppler vibrometer on a moving platform," *Exp. Tech.*, vol. 45, pp. 13–24, Feb. 2021.

[23] K. Kaynardag, C. Yang, and S. Salamone, "A rail defect detection system based on laser doppler vibrometer measurements," *NDT E Int.*, vol. 137, Jul. 2023, Art. no. 102858.

[24] C. Yang, K. Kaynardag, and S. Salamone, "Missing rail fastener detection based on laser doppler vibrometer measurements," *J. Nondestruct. Eval.*, vol. 42, no. 3, Jul. 2023, Art. no. 8.

[25] Y. Zeng, A. Nunez, and Z. Li, "Railway sleeper vibration measurement by train-borne laser doppler vibrometer and its speed-dependent characteristics," *Comput.-Aided Civil Infrastruct. Eng.*, vol. 39, no. 16, pp. 2408–2426, Jan. 2024.

[26] C.-H. Yeh, G. Lee, and C.-Y. Lin, "Robust laser speckle authentication system through data mining techniques," *IEEE Trans. Ind. Inform.*, vol. 11, no. 2, pp. 505–512, Apr. 2015.

[27] M. Schewe and C. Rembe, "Signal diversity for laser-doppler vibrometers with raw-signal combination," *Sensors*, vol. 21, no. 3, Feb. 2021, Art. no. 998.

[28] J. Fang, C. Zhao, X. Lu, W. Xiong, and C. Shi, "Dynamic behavior of railway vehicle-ballasted track system with unsupported sleepers based on the hybrid DEM-MBD method," *Construction Building Mater.*, vol. 394, Aug. 2023, Art. no. 132091.

[29] Railway applications - Track - Track geometry qualit, EN 13848, European Committee for Standardization, 2019.

[30] J. C. Nielsen, E. G. Berggren, A. Hammar, F. Jansson, and R. Bolmsvik, "Degradation of railway track geometry-correlation between track stiffness gradient and differential settlement," in *Proc. Inst. Mech. Eng. Part F, J. Rail Rapid Transit*, 2020, pp. 108–119.